



Impacts of Atlantic meridional overturning circulation weakening on Arctic amplification

Yu-Chi Lee^a, Wei Liu^{a,1}, Alexey V. Fedorov^b, Nicole Feldl^c, and Patrick C. Taylor^d

RESEARCH ARTICLE

Affiliations are included on p. 8.

Edited by Eric Rignot, University of California Irvine, Irvine, CA; received February 2, 2024; accepted August 5, 2024

Enhanced warming of the Arctic region relative to the rest of the globe, known as Arctic amplification, is caused by a variety of diverse factors, many of which are influenced by the Atlantic meridional overturning circulation (AMOC). Here, we quantify the role of AMOC changes in Arctic amplification throughout the twenty-first century by comparing two suites of climate model simulations under the same climate change scenario but with two different AMOC states: one with a weakened AMOC and another with a steady AMOC. We find that a weakened AMOC can reduce annual mean Arctic warming by 2 °C by the end of the century. A primary contributor to this reduction in warming is surface albedo feedback, related to a smaller sea ice loss due to AMOC slowdown. Another major contributor is the changes in ocean heat uptake. The weakened AMOC and its associated anomalous ocean heat transport divergence lead to increased ocean heat uptake and surface cooling. These two factors are inextricably linked on seasonal timescales, and their relative importance for Arctic amplification can vary by season. The weakened AMOC can also abate Arctic warming via lapse rate feedback, creating marked cooling from the surface to lower-to-mid troposphere while resulting in relatively weaker cooling in the upper troposphere. Additionally, the weakened AMOC increases the low-level cloud fraction over the North Atlantic warming hole, causing significant cooling there via shortwave (sw) cloud feedback despite the overall effect of sw cloud feedback being a slight warming of the average temperature over the Arctic.

AMOC | Arctic amplification | climate system modeling

Arctic amplification, characterized by enhanced surface warming in the Arctic compared to the global average, is a prominent phenomenon both observed (1, 2) over the past century and projected by climate models for future climate (3, 4). A wide range of factors, including surface albedo feedback, Planck feedback, lapse-rate feedback, near-surface air temperature inversion, cloud feedback, and atmospheric and oceanic energy transports (5–15), have been proposed to explain Arctic amplification. In particular, Arctic sea ice loss appears to be a necessary condition for the generation of large Arctic amplification, not only because it is directly related to the ice-albedo feedback but also because other feedbacks and processes that intensify surface warming might indirectly contribute to sea ice loss and hence Arctic amplification (6, 16–18). Many of these factors are intrinsically linked to the Atlantic meridional overturning circulation (AMOC) due to the complex interplay between AMOC change and top-of-atmosphere (TOA) radiative feedback, as well as the effect of AMOC change on atmospheric and oceanic energy transports (19), and the interactions between the AMOC and Arctic sea ice (20), and between the AMOC and Arctic amplification (21). Therefore, determining the role of the AMOC in Arctic amplification is of central importance.

The AMOC may have slowed in recent decades (22, 23) and is expected to slow further in the twenty-first century (24). On the other hand, an enhanced ocean heat transport (OHT) into the Arctic has been observed (13, 25, 26) and projected (4, 10), which has been suggested as a contributing factor to Arctic warming (4, 10, 27–29). This increased northern high-latitude OHT is primarily attributed to Atlantic water warming (30–32), as the temperature-driven OHT increase outweighs the circulation-driven OHT decrease. Consequently, from the standpoint of Atlantic-Arctic OHT change, the AMOC's impact on Arctic amplification is essentially attenuated.

While several studies have hinted at the role of ocean circulation in Arctic amplification by comparing fully coupled and slab-ocean model simulations (33, 34), the difference between the two simulation suites includes the effects of both the AMOC and gyre circulations, such as those in the subpolar Atlantic and Arctic. Furthermore, the AMOC has been suggested to be tightly linked to Atlantic subpolar ocean temperatures (28) and

Significance

Arctic amplification, the disproportionate warming of the Arctic compared to the global average, has far-reaching effects on weather patterns, ecosystems, and the carbon cycle. Our research quantifies how changes in the Atlantic meridional overturning circulation (AMOC)—a key component of the global climate system—can influence this phenomenon. We demonstrate that a slower AMOC can moderate the Arctic warming by the end of the twenty-first century, primarily through enhanced reflection of solar energy associated with the reduced Arctic sea ice loss. This finding underscores the influential role of ocean currents in global climate regulation and is vital for formulating effective climate responses to greenhouse gas increases.

Author contributions: W.L. designed research; Y.-C.L. performed research; A.V.F., N.F., and P.C.T. contributed new reagents/analytic tools; Y.-C.L., A.V.F., N.F., and P.C.T. analyzed data; and Y.-C.L., W.L., A.V.F., N.F., and P.C.T. wrote the paper.

The authors declare no competing interest.

This article is a PNAS Direct Submission.

Copyright © 2024 the Author(s). Published by PNAS. This article is distributed under Creative Commons Attribution-NonCommercial-NoDerivatives License 4.0

Although PNAS asks authors to adhere to United Nations naming conventions for maps (https://www.un.org/ geospatial/mapsgeo), our policy is to publish maps as provided by the authors.

¹To whom correspondence may be addressed. Email: wei.liu@ucr.edu.

This article contains supporting information online at https://www.pnas.org/lookup/suppl/doi:10.1073/pnas. 2402322121/-/DCSupplemental.

Published September 16, 2024.

subpolar gyre circulation (35). As a result, it remains unclear how AMOC changes influence Arctic amplification.

To address this scientific question, we isolate and quantify the impact of a weakened AMOC on Arctic amplification within a fully coupled climate system under anthropogenic warming by the end of the twenty-first century. Based on the historical and RCP8.5 (Representative Concentration Pathway 8.5; free-AMOC hereafter) simulations by the Community Climate System Model version 4 (CCSM4), we perform a parallel sensitivity experiment (fixed-AMOC hereafter) with the same model since 1980. This experiment is driven by the same historical and RCP8.5 forcing agents as the free-AMOC simulation but with freshwater gradually removed over the subpolar North Atlantic and uniformly redistributed to the rest of the global oceans (36-39) (Materials and Methods). Due to the freshwater removal, the AMOC strength remains nearly constant since 1980 in the model simulation. This fixed-AMOC simulation shows an insignificant AMOC trend of 0.00 ± 0.03 Sv decade⁻¹ (ensemble mean trend \pm one SD of trends among ensembles, $1 \text{ Sv} = 10^6 \text{ m}^3 \text{ s}^{-1}$) from 1981 to 2100, whereas the free-AMOC experiment shows a significant AMOC decline trend of -0.75 ± 0.03 Sv decade⁻¹ during this period (Fig. 1A). The difference between the free- and fixed-AMOC simulations enables us to elucidate how the weakened AMOC influences Arctic amplification through altering atmospheric energy transport (AET), OHT, and a variety of local physical processes.

Results

The AMOC Impact on the Arctic Amplification. We begin by comparing the changes in surface air temperature over the Arctic ($60^{\circ}N-90^{\circ}N$) between observations and the free-AMOC simulation (*Materials and Methods*). Despite decadal variability, both observations and model simulation display a significant trend of rapid surface warming in the Arctic (Fig. 1*B*). Between 1901 and 2022, observations show a warming trend of 0.17 ± 0.01 °C decade⁻¹ (observational mean trend \pm one SD of trends among observations), while the free-AMOC simulation shows a warming trend of 0.27 ± 0.01 °C decade⁻¹ (ensemble mean trend \pm one SD of trends among ensembles). The overlap of observations and model results suggests that CCSM4 can generally well simulate the observed Arctic warming.

We further examine Arctic surface (2-m) air temperature changes in the two suites of CCSM4 simulations. Between 1981 and 2100, Arctic warming trends are 0.72 ± 0.02 °C decade⁻¹ and 0.85 ± 0.02 °C decade⁻¹ (ensemble mean trend \pm one SD of trends among ensembles) for the free- and fixed-AMOC simulations, respectively. Notably, the free-AMOC simulation reveals a slower warming rate compared to the fixed-AMOC simulation. This difference becomes more pronounced after the 2030s and reaches its peak during the last two decades of the century (Fig. 1*B*). A comparison between the free- and fixed-AMOC simulations reveals approximately 2 °C less

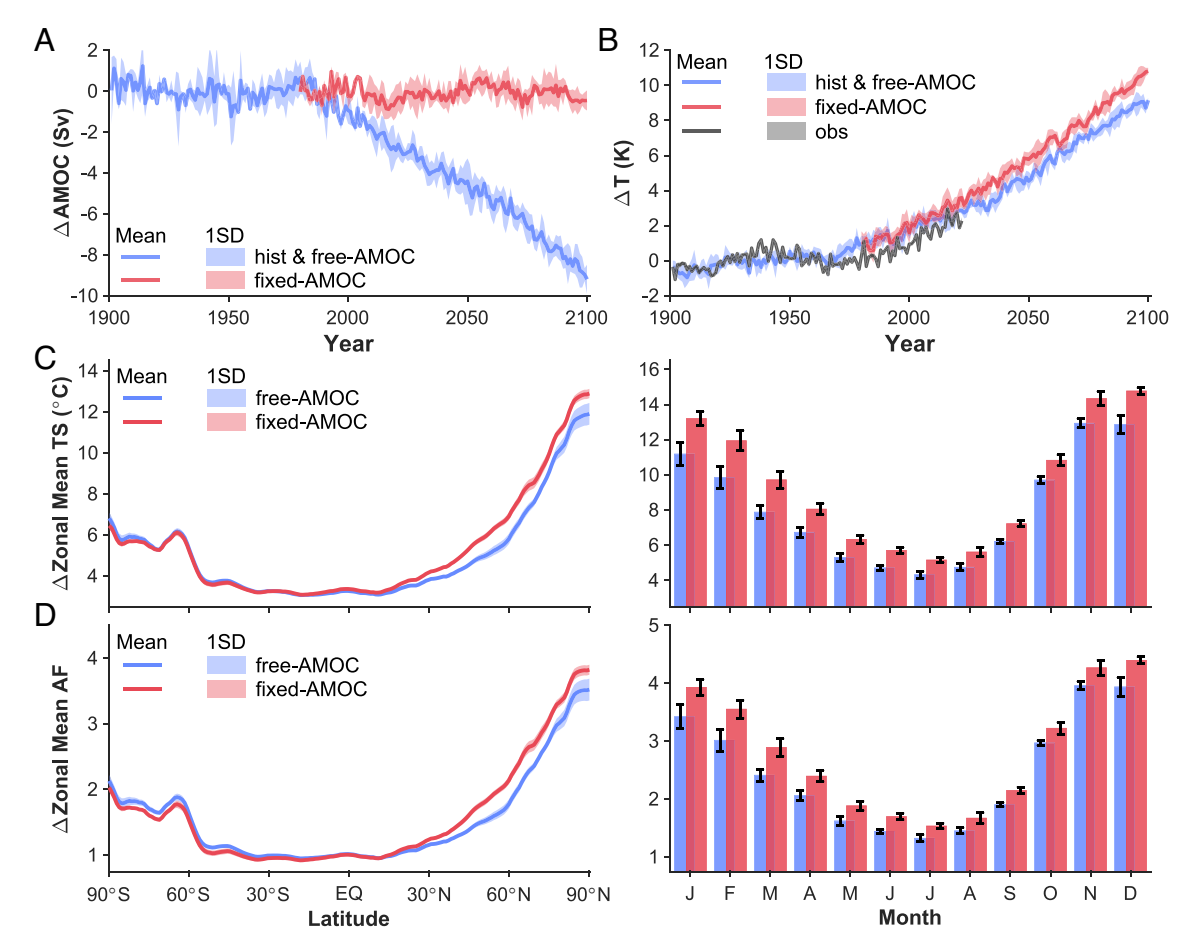


Fig. 1. (*A*) Annual mean AMOC strength anomalies (relative to the average over 1901 to 1980) from the ensemble means of the free- (blue) and fixed-AMOC (red) simulations between 1901 and 2100. (*B*) Annual mean Arctic surface temperature anomalies (relative to the average over 1901 to 1980) from three-observation mean (gray) between 1901 and 2022 and surface (2-m) air temperature anomalies from the ensemble means of the free- (blue) and fixed-AMOC (red) simulations between 1901 and 2100. (*C*) Zonal and annual mean (*Left*) and Arctic-averaged monthly mean (*Right*) surface air temperature anomalies (relative to the average over 1961 to 1980) for the ensemble means of the free- (blue) and fixed-AMOC (red) simulations between 2081 and 2100. (*D*) Same as *C* but with amplification factor (AF), defined as the ratio of temperature changes between each latitude and the tropics (30°S–30°N). In (*A* and *B*) and *Left* panels of (*C* and *D*), lines represent one SD of observation or simulation ensemble members. Error bars on the *Right* panels of (*C* and *D*) represent one SD of the simulation's ensemble members.

warming generally across the Arctic during 2081 and 2100 (Figs. 1B and 2 A and B). This reduced warming, or AMOC-induced anomalous cooling, is particularly striking in the North Atlantic, adjacent to the south of Greenland, often referred to as the North Atlantic warming hole (36) (Fig. 2C). Our findings are further substantiated through the analysis of zonal-averaged surface temperature and Arctic amplification factor (AF) changes (Fig. 1 C and D). The weakened AMOC decelerates Arctic warming by 1.37 °C and reduces the Arctic AF by 0.36 in terms of the annual and ensemble mean. Seasonally, the AMOC-induced cooling is most prominent during the cold seasons from December to March.

Physical Processes in the Diminished Arctic Amplification. To better understand the physical processes by which a weakened AMOC influences Arctic amplification, we use radiative kernels (40) to quantify radiative feedback and partial temperature

contributions (Materials and Methods) to Arctic amplification. The partial temperature contribution is helpful for comparing the relative strengths of feedbacks; however, it is a diagnostic decomposition of the local energy budget, and the warming attributed to any individual feedback need not be realized. This distinction is due to the interactions between feedbacks and with climate system characteristics such as ocean heat content at seasonal scales (41), and the use of transient simulations. Meanwhile, because our simulations are identically forced by anthropogenic factors (i.e., greenhouse gases and aerosols), the radiative forcing cannot explain the different surface temperature responses. As a result, we include the forcing-associated warming in the residual rather than calculating it explicitly, noting that the difference in residuals in Fig. 3C is near zero. Among a variety of factors, we find that surface albedo feedback emerges as the main driver of the annual mean Arctic warming, which, on average,

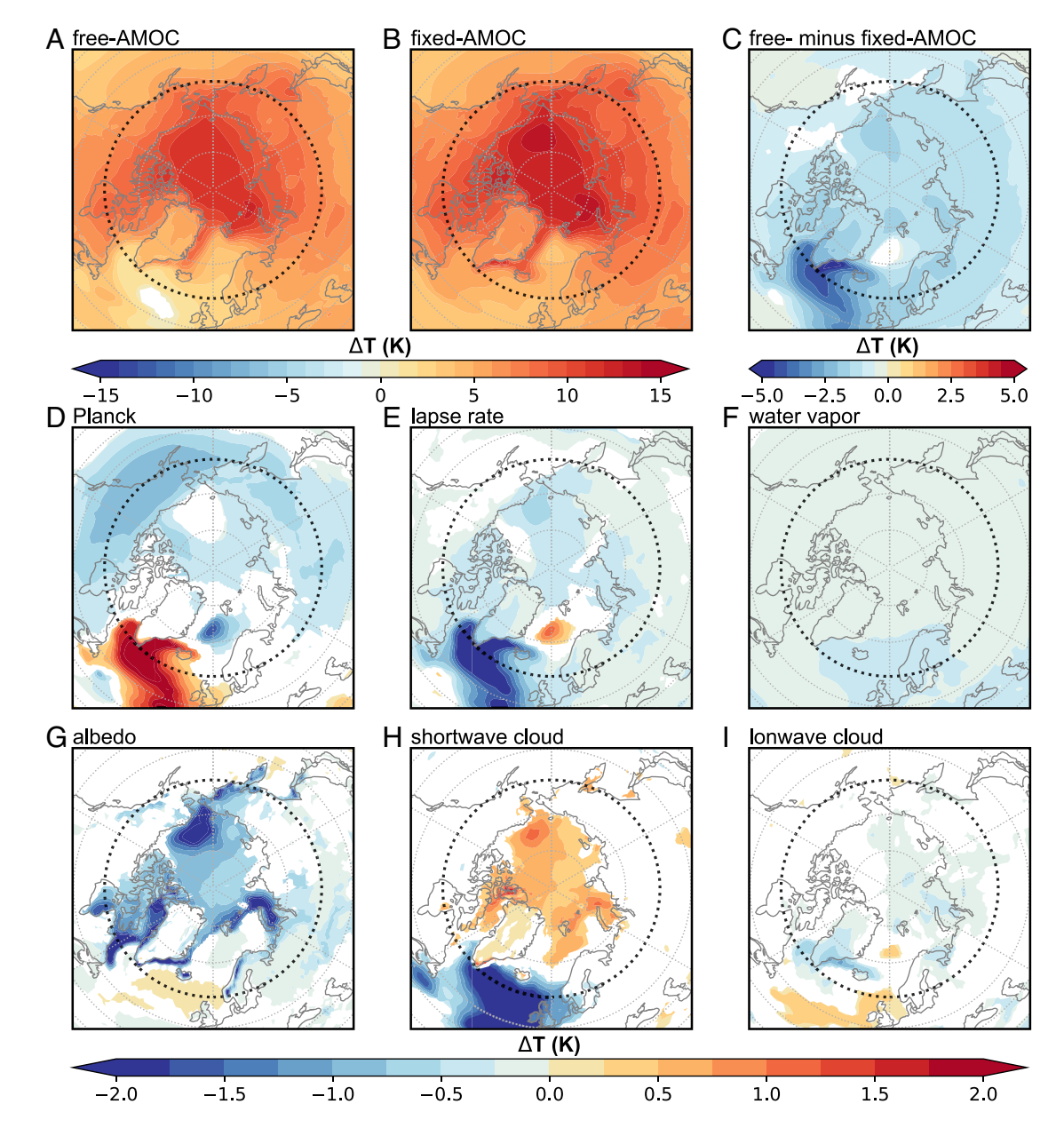


Fig. 2. (A-C) Annual mean surface (2-m) air temperature anomalies (relative to the average over 1961 to 1980) for the ensemble means of the (A) free- and (B) fixed-AMOC simulations between 2081 and 2100 (color shading in K), and (C) the difference (A – B). (D-I) Annual and ensemble mean partial temperature contribution differences between the free- and fixed-AMOC simulations (free- – fixed-AMOC; color shading in K) for (D) Planck response, (E) lapse rate feedback, (F) water vapor feedback, (G) albedo feedback, (H) shortwave cloud feedback, and (I) longwave cloud feedback. In all panels, only differences statistically significant at the 95% confidence level are shown.

explains 3.52 K and 4.12 K of Arctic warming over 2081 to 2100 in the free- and fixed-AMOC simulations, respectively (Fig. 3 *A* and *B*). The surface albedo feedback results from sea ice melting, which decreases surface reflectivity and increases the absorption of solar radiation, thereby warming the surface. Given that feedbacks interact and compensate for one another, while the surface albedo feedback promotes a large radiative response, other processes are crucial in how the surface temperature change manifests, as we will show below.

The extent of the impact of surface albedo feedback closely aligns with the reduction in annual mean Arctic sea ice concentration. Despite Arctic sea ice dwindling in response to global warming in both CCSM4 simulations (SI Appendix, Fig. S1 A and B), the decrease in sea ice cover across the Arctic is 10% less severe for a weakened AMOC than it would be in the case of a fixed AMOC. However, in specific regions adjacent to the Atlantic and central areas between the Beaufort Sea and Chukchi Sea, the lessened sea ice reduction can reach up to 20% (SI Appendix, Fig. S1C). The relatively less abated Arctic sea ice, particularly in regions near the Atlantic, is linked to the weakened Atlantic overturning and associated decrease in the northward OHT (20, 39, 42) across the Atlantic sector (SI Appendix, Fig. S2). The reduced sea ice loss around the Beaufort Sea and Chukchi Sea, on the other hand, is likely linked to air-sea-ice interactions (41) as well as a decrease in the northward OHT through the Bering Strait (41). This is because the weakened AMOC can deepen the Aleutian low during boreal winter via atmospheric teleconnections (36) and hence modify the ocean circulation and heat transport over the Bering Sea. Compared to the fixed-AMOC case, the slowed AMOC diminishes the increase of the northward OHT through the Bering Strait by 0.01 petawatt (PW) between 2081 and 2100 (SI Appendix, Fig. S2). Over the Arctic region, the abated sea ice loss induces approximately 44% (-0.60 K) of the reduced warming, which is primarily attributed to surface albedo feedback (Fig. 3*C*), particularly evident in areas characterized by relatively pronounced reduction of sea ice loss (Fig. 2*G* and *SI Appendix*, Fig. S1*C*).

The AMOC slowdown can also effectively modulate Arctic warming by changing annual mean ocean heat uptake/loss. We find that the weakened AMOC reduces Arctic warming by approximately 34% (-0.47 K) via altering ocean heat uptake/loss over the Arctic Mediterranean (43), making it the second most substantial contributor to the cooling process (Fig. 3C). To elucidate the detailed oceanic cooling process, we calculate the difference in ocean temperature budgets between the free- and fixed-AMOC simulations between 2081 and 2100 (Materials and Methods). We find that a weakened AMOC causes a general OHT divergence and, as a result, a cooling tendency of whole-depth water in the subpolar North Atlantic as well as the Atlantic sector of the Arctic, including the Labrador and Greenland Seas (Fig. 4A). This OHT divergence promotes ocean heat uptake via the ocean surface (Fig. 4B), primarily through turbulent heat flux (36, 44, 45) (SI Appendix, Fig. S8K), but it also dominates the ocean temperature budget, resulting in a net cooling of Arctic waters (Fig. 4C), diminished ocean heat storage, and a lessened sea ice loss in these regions (SI Appendix, Fig. S1C). To counterbalance the AMOCinduced OHT divergence, the ocean responds by absorbing more heat from the atmosphere, thereby engendering a cooling effect on surface temperature. It merits attention that beyond the Labrador and Greenland Seas, the AMOC slowdown may indirectly affect the local processes (17) over the Barents, Kara, and Chukchi Seas, where OHT divergence and ocean heat uptake are also visible (Fig. 4 A and B).

On the other hand, the AMOC-enhanced ocean heat uptake change (Fig. 4E) is much larger in magnitude than the AMOC-induced net TOA radiation change (Fig. 4D), which induces a general convergence of AET over the Arctic, particularly over the North Atlantic warming hole and around the Bering Strait

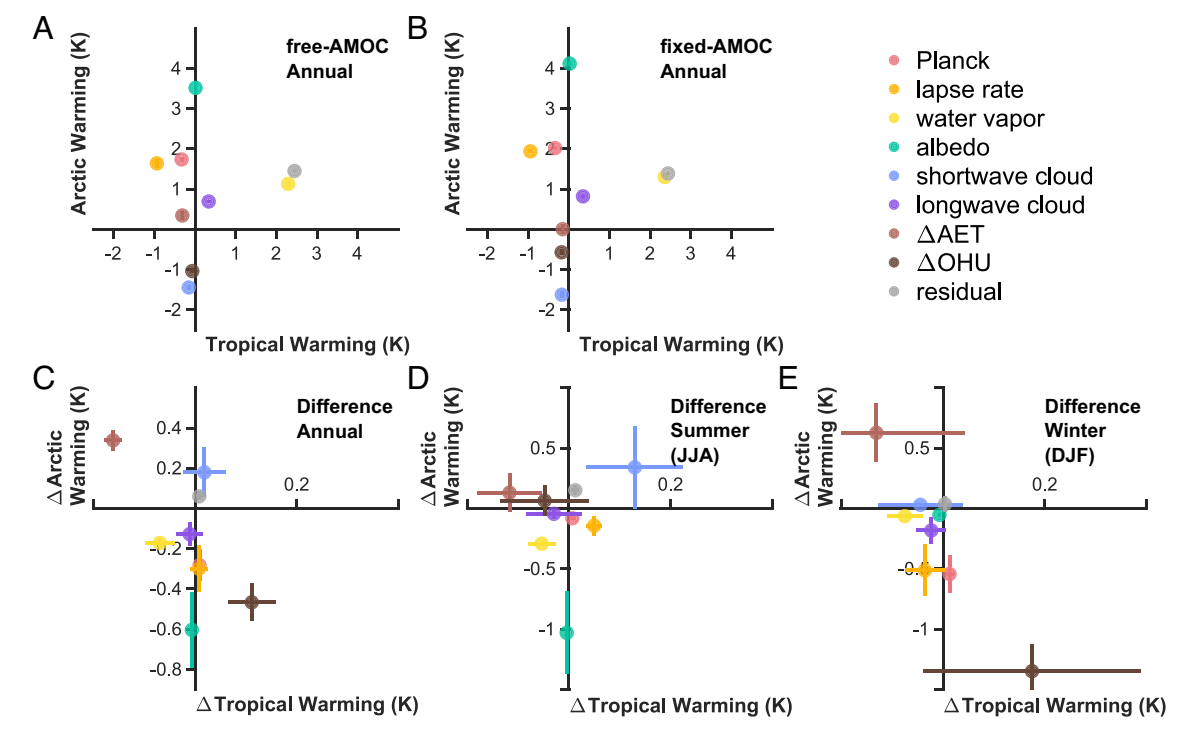


Fig. 3. Partial annual mean surface air temperature changes for the Arctic (60°N–90°N) compared to the tropics (30°S–30°N) from the (*A*) free- and (*B*) fixed-AMOC simulations during 2081 to 2100 compared to 1961 to 1980, and (*C*) AMOC impacts on annual mean temperature changes (free – fixed, A – B). Colored scatters present the partial temperature contributions due to Planck response, the lapse rate, water vapor, shortwave and longwave cloud feedbacks, AET, ocean heat uptake/ loss, and the residual term. (*D* and *E*) Same as (*C*) but for AMOC impacts on boreal (*D*) summer (June-July-August; JJA) and (*E*) winter (December-January-February; DJF) temperature changes. Error bars show the one SD of the differences of five ensemble members between the free- and fixed-AMOC simulations for all panels.

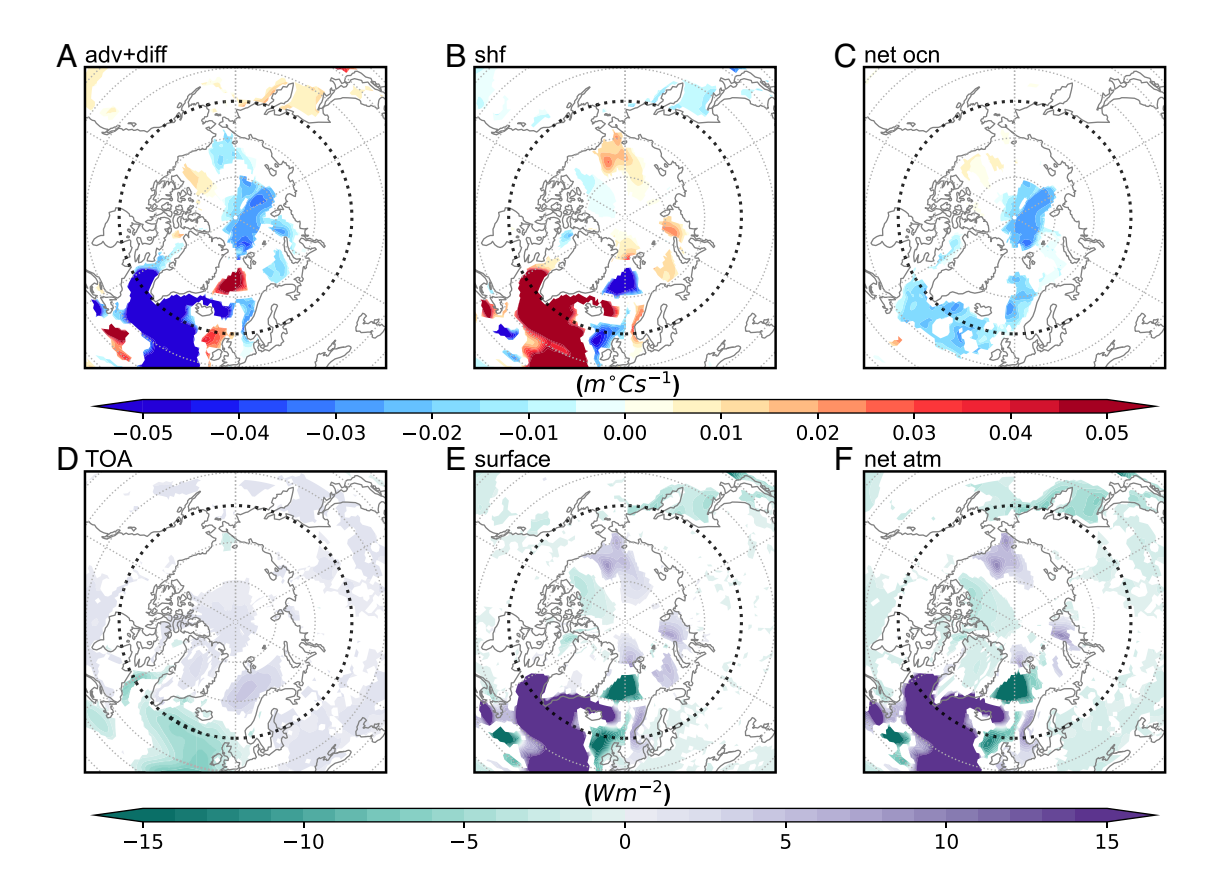


Fig. 4. (A-C) Annual and ensemble mean ocean temperature tendency differences between the free- and fixed-AMOC simulations (free - fixed) during 2081 to 2100 induced by (A) OHT convergence/divergence (convergence positive, divergence negative) and (B) net surface heat flux across ocean surface (downward positive), as well as (C) the net vertically integrated temperature tendency (A plus B). (D-F) Annual and ensemble mean differences between the free- and fixed-AMOC simulations (free – fixed) during 2081 to 2100 for (D) TOA and (E) surface energy fluxes (positive downward), and (F) AET convergence/divergence (E – D; convergence positive, divergence negative). In all panels, only differences statistically significant at the 95% confidence level are shown.

(Fig. 4F). The zonally integrated AET reveals that the weakened AMOC causes an overall net increase in the total AET (Materials and Methods) in the Northern Hemisphere middle and high latitudes, owing primarily to an enhanced (stationary plus transient) eddy energy transport component (SI Appendix, Fig. S2). The increase in the northward AET at 60°N amounts to 0.04 PW, meaning that the AMOC-induced AET change enhances rather than reduces Arctic amplification (Fig. 3C). It is also worth noting the opposite AET and OHT changes caused by AMOC slowdown in the Northern Hemisphere middle and high latitudes (SI Appendix, Fig. S2), which leads to a much smaller change in the total atmospheric and oceanic energy transports and indicates the Bjerknes compensation (19, 46).

The slowed AMOC can also have a significant impact on Arctic amplification via temperature feedback. Specifically, the contributions from vertically uniform temperature change, known as the Planck feedback, are 1.80 K with a weakened AMOC and 2.10 K with a fixed AMOC (Fig. 3 A and B). The Planck feedback promotes warming of the Arctic because the feedback is weaker (i.e., less stabilizing) in the Arctic than in the tropics; it is calculated as a deviation from its global and annual mean (*Materials and Methods*). Contributions arising from deviations from a vertically uniform temperature change, known as the lapse rate feedback, are 1.70 K for the free- and 2.02 K for the fixed-AMOC simulations (Fig. 3 A and B). Collectively, a weakened AMOC could result in approximately 43% (-0.61 K) of the cooling effect in the Arctic due to the total temperature feedback. AMOC-induced changes in the Planck response primarily appear as a surface cooling across the Arctic and its neighboring regions. However, a notable exception is the North Atlantic warming hole, where the Planck response contributes to

an anomalous surface warming (Fig. 2D). This geographic distinction reveals that the Planck response is weaker over the North Atlantic warming hole in the free-AMOC simulation, leading to a more significant anomalous warming effect than in other regions due to the strikingly colder surface temperatures in this area (47). In contrast to the free-AMOC simulation, the Planck response is weaker over the central Arctic in the fixed-AMOC simulation. Despite this difference, the temperature changes caused by the Planck response are largely offset by those caused by the lapse rate feedback. In the North Atlantic warming hole and Beaufort/ Chukchi Sea regions, the surface cooling due to lapse rate feedback highlights an unevenly distributed vertical temperature profile (SI Appendix, Fig. S3). In response to a weakened AMOC, air temperatures show marked cooling in the lower-to-mid troposphere, while the upper troposphere exhibits weaker cooling.

In comparison to the aforementioned factors, AMOC-induced changes in cloud feedback (4%; 0.06 K) and water vapor feedback (12%; -0.17 K) contribute less to Arctic amplification. The cloud feedback, in particular, can be further divided into a shortwave (sw) cloud feedback and a longwave (lw) cloud feedback. A weakened AMOC would add approximately 13% (0.18 K) to Arctic warming via sw cloud feedback in comparison to a fixed AMOC, but this effect is largely compensated by the cooling effect from lw cloud feedback (Fig. 3C). Regardless, the rationale for the warming is that less Arctic sea ice is associated with fewer low clouds (48, 49). Thus, as the AMOC decelerates and sea ice loss becomes less pronounced, the cloud fraction diminishes (SI Appendix, Figs. S1 C and S4 C). In particular, fewer low-level clouds (SI Appendix, Fig. S4C) reduce the amount of sw radiation that is reflected back into space and hence warm the surface of the Arctic.

Additionally, the influences of surface albedo feedback and ocean heat uptake change are inextricably linked on seasonal timescales, such that their relative importance in Arctic amplification may vary by season (7, 17, 41, 50–53). In a warming climate, Arctic surface albedo feedback is especially strong during boreal summer (JJA; SI Appendix, Fig. S5 A and B), when large sea ice reduction (SI Appendix, Fig. S1 D and E) leads to more open ocean, allowing more atmospheric heat (primarily solar energy) to enter and be stored in the central Arctic Ocean (*SI Appendix*, Fig. S9 *A* and *E*). Consequently, ocean heat uptake acts to abate summertime Arctic warming. The stored oceanic heat is released to the atmosphere during boreal winter (DJF), which does not always occur in the same locations as summer solar energy absorption due to horizontal advection of heat in the ocean (17). Wintertime oceanic heat release is particularly prevalent in the Kara, Chukchi, and Beaufort Seas, where significant sea ice loss occurs (SI Appendix, Fig. S10 D and H). Sea ice loss in these regions opens the ocean, exposing warmer ocean surfaces to colder air and creating a large air-sea temperature contrast. As a result, the ocean releases heat to the atmosphere via turbulent heat flux and drives wintertime Arctic warming (SI Appendix, Fig. S10 C and G). It merits attention that the North Atlantic warming hole region experiences persistent anomalous ocean heat uptake (or diminished oceanic heat release) throughout all seasons, differing from the seasonal ocean heat uptake and loss in the central Atlantic.

The AMOC slowdown abates Arctic warming through surface albedo feedback, particularly during boreal summer (Fig. 3 D and E), rather than winter. This is because, while the weakened AMOC mitigates Arctic sea ice loss all year round (36) (SI Appendix, Fig. S1), the Arctic is dark during boreal winter, nearly eliminating surface albedo feedback (SI Appendix, Fig. S5 C and D). Additionally, the AMOC slowdown slightly reduces the cooling effect of ocean heat uptake during boreal summer (Fig. 3D), especially over the central Arctic. However, it dramatically weakens the warming effect in boreal winter, which serves as the strongest AMOC-influencing factor on Arctic surface temperature during this season (Fig. 3*E*). This AMOC effect is achieved through reduced oceanic heat release in the central Arctic and persistent anomalous ocean heat uptake south of Greenland (SI Appendix, Fig. S10L).

Discussion

In summary, we compare CCSM4 free- and fixed-AMOC simulations to determine the impact of a weakened AMOC on Arctic amplification under the RCP8.5 scenario throughout the twentyfirst century. We find that the current and projected AMOC slowdown can reduce surface warming over the Arctic. By the end of the century, the strongest AMOC-induced cooling will appear on the Atlantic sector, with temperature changes reaching 5 °C. This cooling phenomenon is primarily linked to a notable slowing in the loss of Arctic sea ice. Surface albedo feedback is identified as the primary contributor to AMOC-induced cooling, accounting for approximately 44% of the cooling. Modifications in ocean heat absorption and temperature feedback are another way that the AMOC affects Arctic amplification. A weakened AMOC, in particular, brings about a general OHT divergence over the Arctic Mediterranean, causing the ocean to absorb more heat from the atmosphere to compensate for the AMOC-induced OHT divergence, resulting in surface temperature cooling. Surface albedo feedback and ocean heat uptake change are inherently linked on seasonal timescales, with their relative importance in Arctic amplification varying by season (17, 18). Note that the surface albedo feedback and ocean heat uptake change compensate one another

in both free- and fixed-AMOC global warming simulations (Fig. 3 A and B), whereas the difference between the free- and fixed-AMOC simulations shows that both factors collectively contribute to the reduced Arctic warming (Fig. 3*C*). The weakened AMOC can also diminish Arctic warming through lapse rate feedback, causing strong cooling from the surface to the lower-to-mid troposphere while leading to relatively weaker cooling in the upper troposphere. Although changes in sw cloud feedback slightly warm the average surface temperature over the Arctic, they contribute to a strong cooling over the North Atlantic warming hole region due to increased low-level cloud fraction from AMOC slowdown. These results shed light on the intricate mechanisms through which the AMOC exerts a substantial influence on Arctic amplification and advance our understanding of the complex dynamics underlying Arctic climate change.

Materials and Methods

Observed Surface Temperatures. To examine surface temperature changes in the Arctic since 1901, we utilize three distinct observed surface temperature datasets. These datasets include the Goddard Institute for Space Studies Surface Temperature product version 4 from NASA, derived from historical weather station data and ocean data from ships, buoys, and other sensors (54, 55); the National Oceanic and Atmospheric Administration Merged Land Ocean Global Surface Temperature Analysis (NOAAGlobalTemp) that combines long-term sea surface temperature (SST) with land surface temperature datasets, including Extended Reconstructed SST, Global Historical Climatology Network, International Comprehensive Ocean-Atmosphere Data Set-Release 3, and International Arctic Buoy Programme (56); and the Met Office Hadley Centre/Climate Research Unit global surface temperature dataset (HadCRUT5) that is a combination of SST measurements from ships and buoys and near-surface air temperature measurements from weather stations (57). For all three observations, we analyze the monthly surface temperature data using a regular grid of 2×2 for GISTEMP, 5×5 for NOAAGlobalTemp, and HadCRUT5. Our examination covers the period from 1901 to 2022. To establish annual mean anomalies, we calculate deviations from the climatological average between 1901 and 1980.

CCSM4 Simulations. We utilize a five-member ensemble for the broadly used CCSM4 historical and RCP8.5 (free-AMOC) simulations. We especially focus on the historical period of 1961 to 1980 and RCP8.5 period of 2081 to 2100. Based on the free-AMOC simulation, we conduct a parallel sensitivity (fixed-AMOC) experiment with five ensemble members. The fixed-AMOC experiment is branched from the free-AMOC simulation in year 1980 and driven by the same historical and RCP8.5 forcing agents as the free-AMOC simulation onward except with a small amount of freshwater gradually removed over the region covering the north of 50°N in the North Atlantic and the Labrador, Greenland, Iceland, and Norwegian Seas and then uniformly redistributed to the rest of global oceans (see more details in refs. 36-39). This freshwater scheme implemented in the fixed-AMOC experiment maintains a near-constant AMOC strength since 1980. Here, the AMOC strength is defined as the maximum of meridional overturning streamfunction below 500 m in the North Atlantic. We used monthly averaged model data for our analysis.

Radiative Feedback. We apply the radiative kernel technique (58, 59) to calculate the climate feedback (in units of W m⁻² K⁻¹) from a TOA perspective, using CAM5 radiative kernels (40).

The surface albedo feedback is calculated as

$$\lambda_{alb} = \frac{\Delta R_{alb}}{[\Delta T_s]} = K_{alb} \times \frac{\Delta alb}{[\Delta T_s]}.$$
 [1]

The Planck feedback is calculated as

$$\lambda_{plk} = \frac{\Delta R_{plk}}{\left[\Delta T_{s}\right]} = \frac{K_{T_{s}} \times \Delta T_{s} + \int_{p_{0}}^{p} K_{T_{a}} \times \Delta T_{s} dp}{\left[\Delta T_{s}\right]}.$$
 [2]

The lapse rate feedback is calculated as

$$\lambda_{lr} = \frac{\Delta R_{lr}}{\left[\Delta T_{s}\right]} = \frac{\int_{\rho_{0}}^{\rho} K_{T_{a}} \times (\Delta T_{a} - \Delta T_{s}) d\rho}{\left[\Delta T_{s}\right]}.$$
 [3]

The water vapor feedback is calculated as

$$\lambda_{wv} = \frac{\Delta R_{wv}}{\left[\Delta T_{s}\right]} = \frac{\int_{p_{0}}^{p} K_{q} \times \Delta \ln(q) dp}{\left[\Delta T_{s}\right]}.$$
 [4]

The sw and lw cloud feedbacks are calculated as

Ocean Temperature/Heat Budget. We analyze ocean temperature/heat budget, which states that the full-depth integrated ocean temperature tendencies at unit area can be written as

$$tendency_{tot} = tendency_{shf} + tendency_{OHTC},$$
 [8]

where tendency_{tot} denotes the total vertically integrated temperature tendency, tendency_{shf} denotes the temperature tendency induced by surface heat flux, and tendency_{OHTC} denotes the temperature tendency due to OHT convergence/divergence (39). The tendency_{OHTC} is computed using the advection and diffusion of heat in the ocean, which involves both the horizontal and vertical transport of heat by ocean circulations.

Meridional OHT. We calculate the zonally integrated meridional OHT as

$$\lambda_{sw_cld} = \frac{\Delta R_{sw_cld}}{\left[\Delta T_{s}\right]} = \frac{\left[\Delta CRF_{sw} + \left(K_{sw_q}^{cs} - K_{sw_q}\right)\Delta q + \left(K_{a}^{cs} - K_{a}\right)\Delta a + \left(G_{sw}^{cs} - G_{sw}\right)\right]}{\left[\Delta T_{s}\right]},$$
[5]

$$\lambda_{lw_cld} = \frac{\Delta R_{lw_{cld}}}{\left[\Delta I_{s}\right]} = \frac{\left[\Delta CRF_{lw} + \left(K_{lw_{q}}^{cs} - K_{lw_{q}}\right)\Delta q + \left(K_{I_{a}}^{cs} - K_{I_{a}}\right)\Delta I_{a} + \left(K_{I_{s}}^{cs} - K_{I_{s}}\right)\Delta I_{s} + \left(G_{lw}^{cs} - G_{lw}\right)\right]}{\left[\Delta I_{s}\right]}.$$

$$[\mathbf{\delta}]$$

In Eqs. **1–6**, p_0 represents the surface pressure level, p represents the pressure level of tropopause, ΔR represents the change in TOA radiation due to individual feedback (subscript denoting each feedback), K and K^{CS} represent all-sky and clear-sky radiative kernel responses to small perturbations (subscript denoting each perturbation), Δalb represents surface albedo change between 2081 to 2100 and 1961 to 1980, $\Delta T_{\rm S}$ represents surface temperature change, $[\Delta T_s]$ represents zonally averaged surface temperature change (60), ΔT_a represents air temperature change, q represents specific humidity, ΔCRF represents the change in cloud radiative forcing where subscripts denote sw and lw, and G and G^{CS} represent all-sky and clear-sky radiative forcing due to anthropogenic climate change where subscripts denote sw and lw.

Partial Temperature Contribution. We use a local energy budget to convert the energetic contributions of radiative feedback and energy transport anomalies for 2081 to 2100 relative to 1961 to 1980 into contributions to near-surface warming in the tropics (30°S-30°N) and Arctic (60°N-90°N), as in previous studies (8, 11, 60, 61). For each region, the annual mean warming contributions are defined by dividing each term by the global-mean Planck feedback λ_{plk} as

$$\Delta T_{s} = -\frac{\lambda'_{plk} \left[\Delta T_{s} \right]}{\overline{\lambda}_{plk}} - \frac{\sum_{i} \lambda_{i} \left[\Delta T_{s} \right]}{\overline{\lambda}_{plk}} - \frac{\Delta AET}{\overline{\lambda}_{plk}} - \frac{\Delta OHU}{\overline{\lambda}_{plk}} - \frac{\Delta R_{rd}}{\overline{\lambda}_{plk}}, \quad [7]$$

where $[\Delta T_S]$ is the change in zonal-averaged surface air temperature between 2081 to 2100 and 1961 to 1980. $\lambda'_{plk} = \lambda_{plk} - \overline{\lambda_{plk}}$ denotes the difference between the regional, seasonal, and global annual averaged Planck feedback. Δ AET = $\Delta R_{TOA} - \Delta R_{sfc}$, denoting the change in atmospheric energy convergence/ divergence, $\Delta OHU = \Delta R_{sfc'}$ denoting the change of net surface heat flux, and ΔR_{rd} is the residual term that includes the radiative forcing under the historical and RCP8.5 scenarios. $-\frac{\lambda'_{plk}[\Delta^I_s]}{\lambda_{plk}}$ represents the partial temperature contribution due to Planck response. $-\frac{\sum_i \lambda_i \left[\Delta T_s\right]}{\lambda_{plk}}$ represents the partial temperature contributions due to the lapse rate, water vapor, albedo, sw, and lw cloud feedbacks. $-\frac{\Delta AET}{\lambda_{plk}}$ represents the partial temperature contribution due to atmospheric energy convergence/divergence. $-\frac{\Delta OHU}{\lambda_{plk}}$ represents the partial temperature contribution due to ocean heat uptake/loss. $-\frac{\Delta R_{rd}}{\lambda_{plk}}$ represents the partial temperature contribution due to the residual term.

$$OHT = \int_{X_{uv}}^{X_E} \int_{-H}^{0} \rho_0 C_{po} \left[\nabla \cdot \left(\overline{v}_o \theta + v_o^* \theta + D \right) \right] dz dx,$$
 [9]

where X_F and X_W denote the longitudes of the western and eastern boundaries of ocean basin at certain latitude, ho_0 is sea water density, C_{po} is the specific heat of sea water, θ is potential temperature of sea water, and $-\dot{H}$ is ocean depth. ∇ , \bar{v}_{o} and v_a^* are three-dimensional gradient operator and velocity, where \overline{v}_a is Eulerianmean velocity, and v* is the sum of mesoscale and submesoscale eddy-induced velocities. D denotes diffusion and other subgrid processes.

Meridional AET. We calculate the total AET at latitude ϕ as the difference between TOA radiative fluxes R_{TOA} and net surface heat flux R_{sfr}

$$AET = 2\pi a^2 \int_{-\pi/2}^{\phi} \left[R_{TOA} - R_{sfc} \right] cos\phi' d\phi',$$
 [10]

where a is the radius of the Earth, and [.] represents zonal mean. The global averaged imbalance is removed from the integration to ensure the transport is zero at the poles.

We further decompose the total AET into the components induced by mean meridional circulation (MMC) and eddies. The MMC component is calculated from the meridional wind v_a and the moist static energy $h = c_{pa}T_a + L_v q + gZ$, where c_{na} is the specific heat of air at constant pressure, I_a is air temperature, L_v is the latent heat of vaporization of water, q is the acceleration of gravity, and Zis geopotential height. To prevent errors in cases where mass is not conserved in MMC, we remove the weighted vertical average of moist static energy (7).

We calculate the MMC component as

$$MMC = -\frac{2\pi a cos \phi}{g} \int_{\rho_s}^{0} \left[\overline{v_a} \right] \left[\tilde{h} \right] dp, \qquad [11]$$

where p_s is surface pressure and $[\tilde{h}] = [\bar{h}] - \sum_{p_s}^0 [\bar{h}] dp / \sum_{p_s}^0 dp$.

We calculate the eddy component as the difference between the total AET and MMC components,

$$EDDY = AET - MMC.$$
 [12]

Significance Test. The difference between the free- and fixed-AMOC simulations is tested with two-sample Student t-distribution as

$$t = \frac{\overline{x} - \overline{y}}{\sqrt{\frac{s_x^2}{n} + \frac{s_y^2}{n}}},$$
 [13]

where \overline{x} and \overline{y} are the ensemble means, and s_x and s_y are one SD from freeand fixed-AMOC simulations, respectively. n denotes the number of ensemble members for either simulation (five in this study).

- M. C. Serreze, A. P. Barrett, J. C. Stroeve, D. N. Kindig, M. M. Holland, The emergence of surface-based Arctic amplification. Cryosphere 3, 11-19 (2009).
- M. Rantanen et al., The Arctic has warmed nearly four times faster than the globe since 1979. Commun. Earth Environ. 3, 168 (2022).
- S. Manabe, R. J. Stouffer, Sensitivity of a global climate model to an increase of CO₂ concentration in the atmosphere. J. Geophys. Res. Oceans 85, 5529-5554 (1980).
- M. M. Holland, C. M. Bitz, Polar amplification of climate change in coupled models. Clim. Dyn. 21, 221-232 (2003).
- R. Bintanja, R. G. Graversen, W. Hazeleger, Arctic winter warming amplified by the thermal inversion and consequent low infrared cooling to space. Nat. Geosci. 4, 758–761 (2011).
- A. Dai, D. Luo, M. Song, J. Liu, Arctic amplification is caused by sea-ice loss under increasing CO2. Nat. Commun. 10, 121 (2019).
- N. Feldl, S. Po-Chedley, H. K. A. Singh, S. Hay, P. J. Kushner, Sea ice and atmospheric circulation shape the high-latitude lapse rate feedback. NPJ Clim. Atmos Sci. 3, 41 (2020).
- H. Goosse et al., Quantifying climate feedbacks in polar regions. Nat. Commun. 9, 1919 (2018).
- L. C. Hahn, K. C. Armour, M. D. Zelinka, C. M. Bitz, A. Donohoe, Contributions to polar amplification in CMIP5 and CMIP6 models. Front. Earth Sci. (Lausanne) 9, 710036 (2021).
- Y.-T. Hwang, D. M. W. Frierson, J. E. Kay, Coupling between Arctic feedbacks and changes in poleward energy transport. *Geophys. Res. Lett.* **38**, 17 (2011).
- F. Pithan, T. Mauritsen, Arctic amplification dominated by temperature feedbacks in contemporary climate models. Nat. Geosci. 7, 181-184 (2014).
- J. A. Screen, I. Simmonds, The central role of diminishing sea ice in recent Arctic temperature amplification. *Nature* **464**, 1334–1337 (2010).
- R. F. Spielhagen et al., Enhanced modern heat transfer to the Arctic by warm Atlantic water. Science **1979**, 450-453 (2011).
- M. F. Stuecker et al., Polar amplification dominated by local forcing and feedbacks. Nat. Clim. Change 8, 1076-1081 (2018).
- P. C. Taylor et al., Process drivers, inter-model spread, and the path forward: A review of amplified Arctic warming. Front. Earth Sci. (Lausanne) 9, 758361 (2022).
- M. Yoshimori, A. Abe-Ouchi, A. Laîné, The role of atmospheric heat transport and regional feedbacks in the Arctic warming at equilibrium. Clim. Dyn. 49, 3457-3472 (2017).
- 17. A. Dai, M. T. Jenkins, Relationships among Arctic warming, sea-ice loss, stability, lapse rate feedback, and Arctic amplification. Clim. Dyn. 61, 5217-5232 (2023).
- M. Jenkins, A. Dai, The impact of sea-ice loss on Arctic Climate feedbacks and their role for Arctic amplification. Geophys. Res. Lett. 48, e2021GL094599 (2021).
- Q. Yang, Y. Zhao, Q. Wen, J. Yao, H. Yang, Understanding bjerknes compensation in meridional heat transports and the role of freshwater in a warming climate. J. Clim. 31, 4791-4806 (2018).
- W. Liu, A. Fedorov, Interaction between Arctic sea ice and the Atlantic meridional overturning circulation in a warming climate. Clim. Dyn. 58, 1811-1827 (2022).
- $A.\ Dai, Arctic amplification \ is \ the \ main \ cause \ of \ the \ Atlantic \ meridional \ overturning \ circulation$ weakening under large CO₂ increases. Clim. Dyn. 58, 3243–3259 (2022).
- E. Frajka-Williams, Estimating the Atlantic overturning at 26°N using satellite altimetry and cable measurements. Geophys. Res. Lett. 42, 3458-3464 (2015).
- D. A. Smeed et al., The North Atlantic ocean is in a state of reduced overturning. Geophys. Res. Lett.
- **45**, 1527-1533 (2018). W. Weijer, W. Cheng, O. A. Garuba, A. Hu, B. T. Nadiga, CMIP6 Models predict significant 21st century
- decline of the Atlantic meridional overturning circulation. Geophys. Res. Lett. 47, e2019GL086075 (2020). M. Årthun, T. Eldevik, L. H. Smedsrud, Ø. Skagseth, R. B. Ingvaldsen, Quantifying the influence of
- Atlantic heat on barents sea ice variability and retreat. *J. Clim.* **25**, 4736-4743 (2012). M. J. Karcher, R. Gerdes, F. Kauker, C. Köberle, Arctic warming: Evolution and spreading of the 1990s
- warm event in the Nordic seas and the Arctic Ocean. J. Geophys. Res. Oceans 108, 3034 (2003). I. Mahlstein, R. Knutti, Ocean heat transport as a cause for model uncertainty in projected Arctic warming. *J. Clim.* **24**, 1451–1460 (2011).
- J. Marshall et al., The ocean's role in the transient response of climate to abrupt greenhouse gas
- forcing. Clim. Dyn. 44, 2287-2299 (2015). H. A. Singh, P. J. Rasch, B. E. J. Rose, Increased ocean heat convergence into the high latitudes with
- CO₂ doubling enhances polar-amplified warming. Geophys. Res. Lett. 44, 10, 583-10, 591 (2017). T. Koenigk, L. Brodeau, Ocean heat transport into the Arctic in the twentieth and twenty-first century
- in EC-Earth. Clim. Dyn. 42, 3101-3120 (2014). A. Nummelin, C. Li, P. J. Hezel, Connecting ocean heat transport changes from the midlatitudes to
- the Arctic Ocean. Geophys. Res. Lett. 44, 1899-1908 (2017). D. Oldenburg, K. C. Armour, L. A. Thompson, C. M. Bitz, Distinct mechanisms of ocean heat transport into
- the Arctic under internal variability and climate change. Geophys. Res. Lett. 45, 7692-7700 (2018).

Data, Materials, and Software Availability. All study NetCDF data have been deposited in Zenodo (62) (10.5281/zenodo.11229701).

ACKNOWLEDGMENTS. This study has been supported by United States National Science Foundation (OCE-2123422, AGS-2053121, and AGS-2237743). W.L. is also supported by the University of California Regents Faculty Development Award. Y.-C.L. is also supported by the University of California Riverside 2023 Geographer's Scholarship for Global Climate Science and Sustainability. A.V.F. has been supported by United States National Science Foundation Award AGS-2053096 and by the Make Our Planet Great Again program (ANR-18-MPGA-0001, France). N.F. is also supported by United States National Science Foundation Award AGS-1753034.

Author affiliations: ^aDepartment of Earth and Planetary Sciences, University of California Riverside, Riverside, CA 92521; ^bDepartment of Geology and Geophysics, Yale University, New Haven, CT 06511; ^cDepartment of Earth and Planetary Sciences, University of California Santa Cruz, Santa Cruz, CA 95064; and dNASA Langley Research Center, Climate Science Branch, Hampton, VA 23681

- 33. R. Chemke, L. M. Polvani, J. E. Kay, C. Orbe, Quantifying the role of ocean coupling in Arctic amplification and sea-ice loss over the 21st century. NPJ Clim. Atmos. Sci. 4, 46 (2021).
- J. E. Kay et al., The influence of local feedbacks and northward heat transport on the equilibrium Arctic climate response to increased greenhouse gas forcing. J. Clim. 25, 5433-5450 (2012).
- 35. J. H. Jungclaus, K. Lohmann, D. Zanchettin, Enhanced 20th-century heat transfer to the Arctic simulated in the context of climate variations over the last millennium. Clim. Past 10, 2201-2213
- W. Liu, A. V. Fedorov, S.-P. Xie, S. Hu, Climate impacts of a weakened Atlantic meridional overturning circulation in a warming climate. Sci. Adv. 6, eaaz4876 (2020).
- W. Liu, D. Duarte Cavalcante Pinto, A. Fedorov, J. Zhu, The impacts of a weakened Atlantic meridional overturning circulation on ENSO in a warmer climate. Geophys. Res. Lett. 50, e2023GL103025
- X. Ren, W. Liu, The role of a weakened Atlantic meridional overturning circulation in modulating marine heatwaves in a warming climate. Geophys. Res. Lett. 48, e2021GL095941 (2021).
- Y.-C. Lee, W. Liu, The weakened Atlantic meridional overturning circulation diminishes recent Arctic sea ice loss. Geophys. Res. Lett. 50, e2023GL105929 (2023).
- A. G. Pendergrass, A. Conley, F. M. Vitt, Surface and top-of-atmosphere radiative feedback kernels for CESM-CAM5. Earth Syst. Sci. Data 10, 317-324 (2018).
- R. C. Boeke, P. C. Taylor, Seasonal energy exchange in sea ice retreat regions contributes to differences in projected Arctic warming. Nat. Commun. 9, 5017 (2018).
- R. Zhang, Mechanisms for low-frequency variability of summer Arctic sea ice extent. *Proc. Natl. Acad.* Sci. U.S.A. 112, 4570-4575 (2015).
- B. Wilbert Weijer et al., Interactions between the Arctic mediterranean and the Atlantic meridional overturning circulation: A review. Oceanography 35, 118–127 (2022).
- U. Hausmann, A. Czaja, J. Marshall, Mechanisms controlling the SST air-sea heat flux feedback and its dependence on spatial scale. Clim. Dyn. 48, 1297-1307 (2017).
- L. Zhang, W. Cooke, Simulated changes of the Southern Ocean air-sea heat flux feedback in a warmer climate. Clim Dyn. 56, 1-16 (2021).
- J. Bjerknes, "Atlantic air-sea interaction" in Advances in Geophysics, H. E. Landsberg, J. Van Mieghem, Eds. (Elsevier, 1964), pp. 1-82.
- I. Mitevski, Y. Dong, L. M. Polvani, M. Rugenstein, C. Orbe, Non-monotonic feedback dependence under abrupt Co₂ forcing due to a North Atlantic pattern effect. Geophys. Res. Lett. 50, e2023GL103617 (2023).
- P. C. Taylor, S. Kato, K.-M. Xu, M. Cai, Covariance between Arctic sea ice and clouds within atmospheric state regimes at the satellite footprint level. J. Geophys. Res. Atmos. 120, 12656-12678 (2015).
- P. C. Taylor, E. Monroe, Isolating the surface type influence on Arctic low-clouds. J. Geophys. Res. Atmos. 128, e2022JD038098 (2023).
- E.-S. Chung et al., Cold-season Arctic amplification driven by Arctic ocean-mediated seasonal energy transfer. Earths Future 9, e2020EF001898 (2021).
- S. A. Sejas, P. C. Taylor, The role of sea ice in establishing the seasonal Arctic warming pattern. Environ. Res. Clim. 2, 035008 (2023).
- T. A. Shaw, Z. Smith, The midlatitude response to polar sea ice loss: Idealized slab-ocean aquaplanet experiments with thermodynamic sea ice. J. Clim. 35, 2633-2649 (2022).
- P.-C. Chung, N. Feldl, Sea ice loss, water vapor increases, and their interactions with atmospheric energy transport in driving seasonal polar amplification. J. Clim. 37, 2713-2725 (2024). GISTEMP Team, "GISS surface temperature analysis (GISTEMP), version 4. NASA Goddard Institute
- for Space Studies" (2023). https://data.giss.nasa.gov/gistemp/. Accessed 6 June 2023.

 N. J. L. Lenssen *et al.*, Improvements in the GISTEMP Uncertainty Model. *J. Geophys. Res. Atmos.*
- **124**, 6307-6326 (2019). R. S. Vose et al., Implementing full spatial coverage in NOAA's global temperature analysis. Geophys.
- Res. Lett. 48, e2020GL090873 (2021). C. P. Morice et al., An updated assessment of near-surface temperature change from 1850: The
- HadCRUT5 data set. J. Geophys. Res. Atmos. 126, e2019JD032361 (2021). B. J. Soden et al., Quantifying climate feedbacks using radiative kernels. J. Clim. 21, 3504-3520 (2008).
- K. M. Shell, J. T. Kiehl, C. A. Shields, Using the radiative kernel technique to calculate climate feedbacks in NCAR's community atmospheric model. J. Clim. 21, 2269–2282 (2008)
- N. Feldl, G. H. Roe, Four perspectives on climate feedbacks. Geophys. Res. Lett. 40, 4007-4011 (2013).
- P. C. Taylor et al., A decomposition of feedback contributions to polar warming amplification. J. Clim. 26, 7023-7043 (2013).
- Y.-C. Lee et al., Data from "Impacts of Atlantic meridional overturning circulation weakening on Arctic amplification." Zenodo. 10.5281/zenodo.11229701. Deposited 20 May 2024.